Channeling Chaotic Rays into Waveguides for Efficient Collection of Microcavity Emission

Qinghai Song,[1,*] Li Ge,[2] Brandon Redding,[3] and Hui Cao[3]

[1]Department of Electronic and Information Engineering, Shenzhen Graduate School, Harbin Institute of Technology, Shenzhen, 518055, China

[2]Department of Electrical Engineering, Princeton University, Princeton, New Jersey 08544, USA

[3]Department of Applied Physics, Yale University, New Haven, Connecticut 06520-8482, USA

(Received 31 January 2012; published 15 June 2012)

We demonstrate a robust and generic mechanism, which we term "chaos-assisted channeling," to achieve unidirectional output from wave-chaotic microcavities with long-lived resonances. It utilizes the coexistence of regular and chaotic ray dynamics in most deformed microcavities. Long-lived resonances are formed by total internal reflection on classical periodic orbits, and their leakage into the chaotic region of the phase space is efficiently channeled into an attached waveguide without additional loss. We explain this behavior using a ray dynamics analysis which is confirmed via numerical simulations and experimental demonstration.

DOI: 10.1103/PhysRevLett.108.243902 PACS numbers: 42.55.Sa, 05.45.Mt, 42.25.−p, 42.60.Da

Photonic circuits (PCs) are envisaged as key elements in fiber-optic communications and photonic computing [1]. Various building blocks of PCs are interconnected by low-loss optical waveguides that offer a high degree of integrability. A promising candidate for compact coherent light sources in PCs is the microdisk laser due to its small footprint [2,3], high quality (Q) factor [4,5], and planar geometry [4,5]. Microdisk lasers exploit total internal reflection (TIR) of light to achieve an extremely high $Q \equiv \omega\tau$ (ω is the resonant frequency and τ the photon lifetime). A Q-factor as high as 10^6 has been obtained in a micron-size GaAs microdisk cavity [5], and it increases to about 10^8 in a 120 μm silica disk [4]. Such high Q-factors lead to ultralow lasing thresholds, which cannot be achieved by Fabry–Perot-based lasers of comparable size. Microdisk cavities have also triggered intense research attention in cavity quantum electrodynamics [6], quantum chaos [7], and as single-photon emitters [8].

There is, however, an important limitation of microdisk lasers due to their rotational symmetry: the output of a microdisk laser is isotropic and cannot be collected efficiently. Earlier attempts to address this issue involve positioning a waveguide in close proximity to the microdisk [4,9–11], but such coupling requires precise alignment. Another approach is to tailor the cavity's geometry to achieve directional output without using waveguide [12–17], also known as "phase space engineering." The introduction of smooth deformations results in high-Q modes with directional outputs [18–21]. Although clever designs can produce emission in a single direction [20] and reduce the in-plane divergence angle of the output beam to a few degrees [22], the out-of-plane divergence is usually very large since the thickness of the microdisk is comparable to or smaller than the wavelength. Coupling the emission to other on-chip devices requires additional collection techniques and generally introduces large insertion loss. A third approach is to attach a waveguide directly to the microdisk which effectively transports the emission to on-chip PCs [23–26]. Unfortunately, the breakdown of TIR at the joint causes significant Q-spoiling. Therefore, finding a strategy to efficiently collect and route the emission while maintaining the high Q-factor is of central importance to the application of microdisk lasers in integrated PCs.

In this Letter, we introduce a novel, robust, and general mechanism that enables ultrahigh Q-factors and unidirectional output from microdisks. It combines the advantages of previous attempts while eliminating their limitations and compromises, and we term it "chaos-assisted channeling" (CAC). The first element of CAC is a deformed microdisk cavity in which ray dynamics is mixed with regular and chaotic motions [12,13]. High-Q resonant modes correspond to regular dynamics along geometric orbits, and in classical ray optics, light in these modes is confined perfectly by TIR and no emission is allowed. In wave optics, the picture is corrected by the inclusion of evanescent escaping due to the curvature of the boundary and "chaos-assisted emission" originated from regular-to-chaos tunneling [12,27,28]. The second element of CAC is a waveguide connected to the deformed cavity. For the orbits that do not overlap with the intersection of the cavity and the waveguide, their high Q-factors are largely unaffected, while their emissions are now channeled efficiently to the waveguide, leading to a unidirectional guided output.

Due to the strong index guiding of light in the disk plane, microdisk cavities are usually treated as a two-dimensional system using the effective refractive index n. From the practical point of view, the most interesting properties of microdisk cavities are their resonant spectra, mode structures, and far-field patterns (FFPs). Extensive research has been conducted in this direction [12,13,28] which also connects to the underlying ray dynamics inside a given cavity. In classical ray optics, light is confined by TIR until

it escapes refractively when its incident angle χ becomes larger than the critical angle $\chi_c \equiv \sin^{-1}(1/n)$. With the exceptions of the circle and ellipse, such ray dynamics are nonintegrable, leading to chaotic or partially chaotic motions; they can be conveniently visualized in the two-dimensional phase space, the Poincaré surface of section (SOS; see Fig. 1), which records the angular momentum $\sin\chi$ and azimuthal angle ϕ each time a ray impinges on the cavity boundary.

Here, we take the example of the quadrupolar deformation $r(\theta) = R(1 + \varepsilon\cos 2\theta)$ and briefly review the properties of the SOS (see more examples in the Supplemental Material [29]). At $\epsilon = 0$, the cavity is circular and the angular momentum is conserved. Each ray follows a horizontal line in the SOS unless it forms a (closed) period-p orbit when $\chi = (p-2)\pi/2p$. Such orbits are known as "whispering-gallery" (WG) modes when $\chi \to \pi/2$. As ε becomes nonzero, the ray dynamics do not become completely chaotic immediately, which would otherwise leave the SOS with random points. Instead, the SOS is mixed with regular and chaotic regions. It consists of unbroken curves close to $\sin\chi = 1$, representing quasi-WG modes, and partially chaotic regions at small $\sin\chi$ [see Fig. 1(a)] [13,30]. Closed curves start to appear in the SOS representing stable periodic motions around simple period-p orbits; these "islands" are surrounded by chaotic regions.

As noted, high-Q resonant modes are formed by TIR and they correspond to classical orbits. The Fresnel relation at a curved interface is modified, and light has a finite probability of tunneling out of the cavity even if the incident angle is above the critical angle [31]. However, since the incident angles of these orbits (especially the quasi-WG modes) are high above the critical angle, the refractive escape at the bouncing points on the boundary is very small [32]. Thus the emission process is dominated by the chaos-assisted emission [12,27,28], which consists of three steps: (1) the light tunnels from the stable islands into the chaotic sea around them then (2) slowly diffuses to the lower part of the SOS until (3) it reaches the leaky region below the critical line which leads to refractive escape. The chaotic diffusion is determined by the unstable manifolds of short periodic orbits (p small), which typically leads to multiple output beams [12,13,20,21].

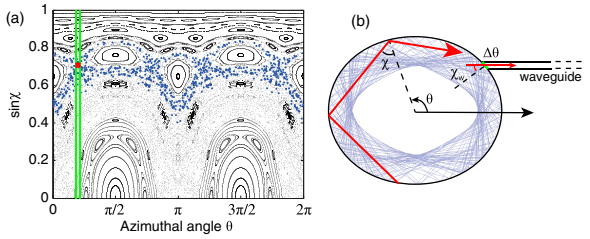

FIG. 1 (color online). (a) Poincaré SOS for a quadruple cavity at $\epsilon = 0.08$. The cavity is taken to be closed. Fine details of the SOS are removed for clarity. Light in a high-Q mode undergoes chaotic motion once it tunnels from islands into the neighboring chaotic region. The first 800 bounces of a typical trajectory outside the period-4 "diamond" islands are indicated by the blue dots, which form a chaotic layer around the islands. Its real space representation is shown in (b). Vertical solid lines in (a) indicate the position of the exit window [joint position between waveguide and cavity in (b)] centered at $\theta = 0.633$ with an angular width of $\Delta\theta = 0.125$. Red square in (a) marks the incident angle χ_w of the light that enters straight into the waveguide.

Once an additional exit port is introduced by the attachment of a waveguide to the cavity boundary, the escape mechanism is fundamentally altered. Assuming the refractive index of the waveguide is the same as the cavity, each time a ray impinges on the exit port, it has a large probability of escaping from the cavity and propagating inside the waveguide. Two main consequences then follow. First, quasi-WG modes with $\chi \sim \pi/2$ are no longer the modes with the highest Q-factor; instead, the short periodic orbits whose bouncing points do not overlap with the exit port become the highest-Q modes [see Fig. 3(a)]. Second, the escape route of the chaotic rays is changed since they can now escape before reaching the critical line in the SOS. The motion of the rays that tunnel out of the islands to the chaotic sea can be described by an intermediate slow horizontal diffusion (in θ) surrounding their original orbits that leads to a chaotic layer (see Figs. 1 and 3), followed by a fast vertical diffusion (in $\sin\chi$) to the critical line that results in refractive escape. The slow horizontal diffusion can be intercepted by the new leak channel (Figs. 1 and 3) above the critical line; thus, most chaotic rays will be collected by the waveguide before refractive escape occurs.

Our proposed scheme is fundamentally different from the previously established escape mechanism which relies on the chaotic diffusion to the critical line for refractive escape. The new mechanism utilizes the slow diffusion surrounding the stable islands to intercept the rays by the waveguide and channel them out. To confirm that the waveguide does intercept most of the tunneled light from the islands, we computed the survival probability calculated from an ensemble of rays starting uniformly above the critical angle in the SOS (see Fig. 2). Each ray is assigned the same initial intensity, which reduces according to the modified Fresnel law [31]. By comparing the total intensities within the exit window and below the critical angle, we conclude that the majority of emission happens via CAC, i.e., via coupling through the exit window into the waveguide.

One significant advantage of our approach is that it is much less sensitive to the cavity shape and applicable to a wide variety of cavity geometries (see the Supplemental Material [29]). The robustness of CAC against a change in the cavity shape is confirmed in our numerical simulation, where we changed the deformation parameter of the quadruple cavity from 0.06 to 0.12 and the waveguide collection efficiency stayed nearly constant at ~90%

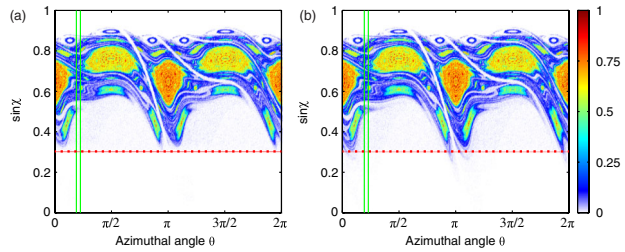

FIG. 2 (color online). Normalized survival probability for (a) transverse electric (TE) and (b) transverse magnetic (TM) polarization in cavity-waveguide system as Fig. 1(b) with $n = 3.3$. We start 40 000 rays of equal intensity start uniformly above the critical angle in the SOS and their intensity evolves by the modified Fresnel law [31]. For simplicity, we reduce the intensity of each ray to zero once it impinges on the exit window. Color represents the total intensity of rays in a tiny area around each point in the SOS. The vertical solid lines and horizontal dotted line indicate the exit window to the waveguide and the critical line, respectively.

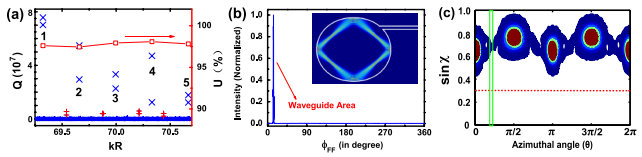

FIG. 3 (color online). (a) Resonance spectrum of the cavity-waveguide system shown in Fig. 1(b). Diamond modes are indicated by × and the others are marked by +. They appear as quasidegenerate pairs due to the slightly different influences of the waveguide on modes of different quasireflection symmetry. Open squares show the unidirectionality (U) of modes 1–5. (b) FFP of mode 4 measured at $r = 2.3R$ as a function of the observation angle ϕ_{FF}. Inset: Corresponding mode structure ($|H_z|$). (c) Enhanced Husimi projection of mode 4. Vertical solid lines indicate the exit windows to the waveguide.

[29]. This is in contrast to the refractive escape via the unstable manifolds, which is shown to be very sensitive to the cavity shape [21].

To confirm that our mechanism inspired by ray analysis is not affected by various wave effects, we calculate the resonant modes of the same quadrupole cavity [29]. Figure 3(a) shows the resonance spectrum of the TE modes and several types of resonances can be identified. The equally-spaced modes 1–5 are the diamond modes localized in the period-4 islands, determined from the mode spacing and field patterns. The diamond modes exhibit the highest Q-factors ($\sim 10^7$–10^8 at $kR \sim 70$), in agreement with our ray analysis. As a comparison, the quasi-WG modes localized along the cavity boundary only have a Q-factor on the order of 10^3 due to the breakdown of TIR at the exit window. Compared to the same cavity without a waveguide, the Q-factors for the diamond modes are reduced by a factor of 10–100 by the waveguide insertion, while the quasi-WG modes experience more than 8 orders of magnitude reduction in Q because they are seriously disturbed by the waveguide. The small reduction of Q for the diamond modes indicates that direct tunneling from the period-4 islands to the exit window is weak, which is further confirmed by changing the separation distance between the stable islands and the exit window (see the Supplemental Material [29]).

Diamond modes 1–5 all have similar FFPs, with the intensity along the waveguide two orders of magnitude larger than the emission into free space. We measure the unidirectionality of modes 1–5 by U (percentage of emission along the waveguide), which indicates that more than 95% of the emission is collected by the waveguide [see Fig. 3(a)]. This is a direct confirmation that CAC is indeed the main emission mechanism in our cavity-waveguide system. To further support this claim, we project the internal mode structure onto the SOS using the Husimi function [30,33]. The enhanced view shown in Fig. 3(c) shows that the tunneled light forms a chaotic layer which is intercepted by the exit window before it reaches the leaky region below the critical line. The integrated intensity across the exit window into the waveguide is one order of magnitude stronger than that below the critical line. We note that the projection intensity on the period-4 islands is much larger than that in the chaotic sea, similar to the case in the absence of the waveguide. This is an evidence that the waveguide doesn't influence the confined motion of the diamond mode on the period-4 islands where the high Q-factor originates. All the above observations hold true for the TM polarization as well.

Besides being insensitive to the wavelength [see Fig. 3(a)] and cavity shape, the CAC is also applicable to a wide range of the refractive index. For a high refractive index where the critical line is far away from stable islands [see Fig. 1(b)], a small change to the position of the critical line will not significantly increase the probability of refractive escape along the unstable manifolds, thus not affecting the measure of unidirectional emission U. As the refractive index decreases, the critical line gradually approaches the short period islands. Once it cuts into the chaotic "layer" where the initial dynamics after the regular-to-chaos tunneling happens, refractive escape becomes more significant and dramatically reduces the percentage of light that would have been channeled into the waveguide (U). This happens around $n = 2$ for the diamond orbit as can be seen from Fig. 1(a), which correlates perfectly with the sudden decrease in U shown in Fig. 4(b). Meanwhile, as the evanescent tunneling of the periodic orbit increases exponentially with the reduction of the distance to the critical angle, it gradually becomes comparable to the regular-to-chaos tunneling and causes a drop in the Q-factor [see Fig. 4(a)]; this process also further reduces the unidirectionality. In this example, we see that CAC leads to a unidirectional emission ($U > 80\%$) over a wide range of refractive index values (from $\sim$2 to 3.9), indicating that our mechanism is robust and can be exploited in most semiconductor materials, ranging from GaN to GaAs. Tailoring the cavity shape can

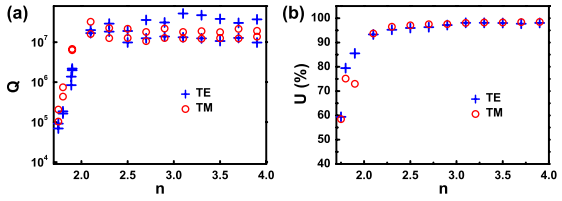

FIG. 4 (color online). Q-factor (a) and unidirectionality U (b) of mode 4 in Fig. 3(a) as a function of the refractive index.

push the lower limit further to $n = 1.5$ for polymer materials (Supplemental Material [29]).

We finally demonstrate the CAC emission mechanism experimentally by fabricating a GaAs microdisk with embedded InAs quantum dots as the gain media [2]. The inset in Fig. 5(a) shows the top-view scanning electron microscope (SEM) image, which matches the designed cavity shape well with $R = 3$ μm. Lasing is confirmed by the observation of the threshold behavior and line narrowing, similar to that reported in Ref. [2]. A typical lasing spectrum, shown in Fig. 5(a), is recorded at the pump power of 900 μJ. It consists of three main peaks at $\lambda = 951, 963$, and 977.5 nm. The same peaks are observed close to the laser threshold, which confirms that they are the diamond modes with the highest Q-factors (see the Supplemental Material [29]). We note that the mode spacing is smaller than the calculated value from a fixed n; this is due to the strong dispersion of the refractive index similar to Ref. [34].

The FFPs of lasing modes are recorded by fabricating a large ring structure enclosing the microdisk cavity and the waveguide (see Fig. 5(b)). We find that all lasing modes produce similar unidirectional outputs along the waveguide, which is consistent with both the ray analysis and the numerical calculation. The relatively broad in-plane divergence angle is caused by the limited resolution of the experimental images. Considering the strong material dispersion present, our experimental results also demonstrate the robustness of the CAC with respect to the emission wavelength and refractive index.

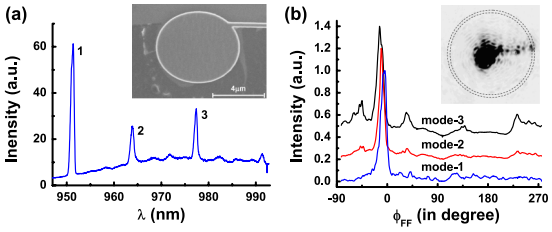

FIG. 5 (color online). (a) Measured emission spectrum from a quadruple-shaped microdisk with a waveguide. Inset: top-view SEM image. (b) Measured FFPs of the three lasing modes shown in (a). Top two lines of mode 2 and mode 3 are shifted vertically 0.2 and 0.4 for clarity, and each line is normalized by its peak intensity. Inset: top-view microscope image of mode 1. Dark regions indicate strong intensity and the dashed ring shows the position of the measurement ring, the scattering from which is measured to give the emission pattern.

To increase the collection efficiency, we can use multiple waveguides positioned between the bouncing points. Our numerical simulation shows that the percentage of the emission collected by the waveguides increases from 88% for a single waveguide to 99% for four waveguides (Supplemental Material [29]). Furthermore, the CAC can be extended to scar modes in chaotic cavities. The scar modes are localized along unstable periodic orbits (UPOs), and waveguides can be placed in between the bounces to intercept the diffused rays [29]. However, the Q-factors may not be as high as the modes on the stable periodic orbits and the waveguide collection efficiency may be lower if the UPOs are close to the critical line.

In summary, we have developed a new and robust mechanism that can be used to generate unidirectional outputs from ultrahigh-Q modes in chaotic microcavities. By adding a waveguide to a deformed microdisk whose emission would otherwise be dominated by chaos-assisted emission, unidirectional emission can be obtained from long-lived resonances. The emission from the microdisk is well guided both in plane and vertically by the waveguide and can be easily integrated into PCs. The demonstrated mechanism is a generic approach to obtain unidirectional emission and low threshold from deformed cavities, as long as short periodic high-Q modes exist surrounded by a chaotic region in the SOS [29]. The Q-factors of long-lived resonances can be optimized to be around half of the values without an attached waveguide ($> 10^8$) while maintaining the unidirectional outputs. And the collection efficiency can be optimized to be more than 99% by adding more waveguides.

We acknowledge Glenn S. Solomon for the molecular beam epitaxy growth of the wafer. This work is supported partly by the open project of the State Key Laboratory on Integrated Optoelectronics No. 2011KFB005, SZ Key Lab of Wind Power and Smart Grid (CXB201005250025A), NSF under the Grants No. ECCS-1068642 and ECCS-1128542. Facilities use was supported by YINQE and NSF MRSEC DMR 1119826.

*qinghai.song@hitsz.edu.cn

[1] P. J. Shadbolt, M. R. Verde, A. Peruzzo, A. Politi, A. Laing, M. Lobino, J. C. F. Matthews, M. G. Thompson, and J. L. O'Brien, Nat. Photonics **6**, 45 (2011).
[2] Q. H. Song, L. Ge, A. D. Stone, H. Cao, J. Wiersig, J.-B. Shim, J. Unterhinninghofen, W. Fang, and G. S. Solomon, Phys. Rev. Lett. **105**, 103902 (2010).
[3] K. Srinivasan, M. Borselli, O. Painter, A. Stintz, and S. Krishna, Opt. Exp. **14**, 1094 (2006).
[4] T. J. Kippenberg, J. Kalkman, A. Polman, and K. J. Vahala, Phys. Rev. A **74**, 051802(R) (2006).
[5] C. P. Michael, K. Srinivasan, T. J. Johnson, O. Painter, K. H. Lee, K. Hennessy, H. Kim, and E. Hu, Appl. Phys. Lett. **90**, 051108 (2007).

[6] E. Peter, P. Senellart, D. Martrou, A. Lemaître, J. Hours, J. M. Gérard, and J. Bloch, Phys. Rev. Lett. **95**, 067401 (2005).
[7] F. Haake, *Quantum Signatures of Chaos* (Springer-Verlag, Berlin, 2000).
[8] D. Press, S. Gotzinger, S. Reitzenstein, C. Hofmann, A. Loffler, M. Kamp, A. Forchel, and Y. Yamamoto, Phys. Rev. Lett. **98**, 117402 (2007).
[9] B. E. Little, J. S. Foresi, G. Steinmeyer, E. R. Thoen, S. T. Chu, H. A. Haus, E. P. Ippen, L. C. Kimerling, and W. Greene, IEEE Photon. Tech. Lett. **10**, 549 (1998).
[10] F. Ou, X. Li, B. Liu, Y. Huang, and S. T. Ho, Opt. Lett. **35**, 1722 (2010).
[11] J. P. Zhang, D. Y. Chu, S. L. Wu, W. G. Bi, R. C. Tiberio, C. W. Tu, and S. T. Ho, IEEE Photon. Technol. Lett. **8**, 968 (1996).
[12] J. U. Nöckel and A. D. Stone, Nature (London) **385**, 45 (1997).
[13] C. Gmachl, F. Capasso, E. E. Narimanov, J. U. Nöckel, A. D. Stone, J. Faist, D. L. Sivco, and A. Y. Cho, Science **280**, 1556 (1998).
[14] A. Mekis, J. U. Nöckel, G. Chen, A. D. Stone, and R. K. Chang, Phys. Rev. Lett. **75**, 2682 (1995).
[15] E. E. Narimanov, G. Hackenbroich, P. Jacquod, and A. D. Stone, Phys. Rev. Lett. **83**, 4991 (1999).
[16] T. Tanaka, M. Hentschel, T. Fukushima, and T. Harayama, Phys. Rev. Lett. **98**, 033902 (2007).
[17] G. D. Chern, H. E. Tureci, A. D. Stone, R. K. Chang, M. Kneissl, and N. M. Johnson, Appl. Phys. Lett. **83**, 1710 (2003).
[18] S.-B. Lee, J.-H. Lee, J.-S. Chang, H.-J. Moon, S. W. Kim, and K. An, Phys. Rev. Lett. **88**, 033903 (2002).
[19] Y. Baryshnikov, P. Heider, W. Parz, and V. Zharnitsky, Phys. Rev. Lett. **93**, 133902 (2004).
[20] J. Wiersig and M. Hentschel, Phys. Rev. Lett. **100**, 033901 (2008).
[21] H. G. L. Schwefel, N. B. Rex, H. E. Tureci, R. K. Chang, A. D. Stone, T. Ben-Messaoud, and J. Zyss, J. Opt. Soc. Am. B **21**, 923 (2004).
[22] Q. J. Wang *et al.*, Proc. Natl. Acad. Sci. U.S.A. **107**, 22407 (2010).
[23] M. Bayer, T. Gutbrod, J. P. Reithmaier, A. Forchel, T. L. Reinecke, P. A. Knipp, A. A. Dremin, and V. D. Kulakovskii, Phys. Rev. Lett. **81**, 2582 (1998).
[24] Y. Z. Huang, K. J. Che, Y. D. Yang, S. J. Wang, Y. Du, and Z. C. Fan, Opt. Lett. **33**, 2170 (2008).
[25] Y. D. Yang, S. J. Wang, and Y. Z. Huang, Opt. Express **17**, 23010 (2009).
[26] G. D. Chern, G. E. Fernandes, R. K. Chang, Q. Song, L. Xu, M. Kneissl, and N. M. Johnson, Opt. Lett. **32**, 1093 (2007).
[27] V. A. Podolskiy and E. E. Narimanov, Opt. Lett. **30**, 474 (2005).
[28] S. Shinohara, T. Harayama, T. Fukushima, M. Hentschel, T. Sasaki, and E. E. Narimanov, Phys. Rev. Lett. **104**, 163902 (2010).
[29] See Supplemental Material at http://link.aps.org/supplemental/10.1103/PhysRevLett.108.243902 for more examples and experimental data.
[30] H. E. Türeci, H. G. L. Schwefel, P. Jacquod, and A. D. Stone, Prog. Opt. **47**, 75 (2005).
[31] M. Hentschel and H. Schomerus, Phys. Rev. E **65**, 045603 (R) (2002).
[32] H. E. Tureci and A. D. Stone, Opt. Lett. **27**, 7 (2002).
[33] M. Hentschel, H. Schomerus, and R. Schubert, Europhys. Lett. **62**, 636 (2003).
[34] M. Lebental, N. Djellali, C. Arnaud, J.-S. Lauret, J. Zyss, R. Dubertrand, C. Schmit, and E. Bogomolny, Phys. Rev. A **76**, 023830 (2007).